Crystal Growth of Two New Niobates, La_2KNbO_6 and Nd_2KNbO_6: Structural, Dielectric, Photophysical, and Photocatalytic Properties

Irina P. Roof,[†] Sangmoon Park,[†] Tom Vogt,[†] Vitaly Rassolov,[†] Mark D. Smith,[†] Shobit Omar,[‡] Juan Nino,[‡] and Hans-Conrad zur Loye*,[†]

University of South Carolina, Columbia, South Carolina 29208, and University of Florida, Gainesville, Florida 32611

Received December 6, 2007. Revised Manuscript Received February 15, 2008

Single crystals of La_2KNbO_6 and Nd_2KNbO_6, space group $C2/m$, $a = 12.746(2)$ Å, $b = 5.7906(1)$ Å, $c = 8.8719(2)$ Å, $\beta = 105.965(1)°$ and $a = 12.545(3)$ Å, $b = 5.6985(1)$ Å, $c = 8.7196(2)$ Å, $\beta = 105.803(1)°$, respectively, were grown out of a reactive hydroxide melt. The two niobates crystallize in a new structure type in which niobium is located in a rare 5-coordinate, square pyramidal coordination environment. La_2KNbO_6 exhibits room-temperature photoluminescence with bright blue emission upon excitation at 260 nm. Semiempirical PM6 calculations were performed to better understand the origin of the photoluminescence. The dielectric properties of La_2KNbO_6 were measured from −150 to 200 °C at four different frequencies. Finally, to assess the photocatalytic properties of La_2KNbO_6, the photocatalytic degradation of methylene blue by La_2KNbO_6 was determined.

Introduction

Complex oxides of niobium comprise a large group of compounds that are known to exhibit a variety of properties, including high dielectric constants[1–5] and photocatalytic behavior,[6–14] which are greatly dependent on the specific crystal and electronic structure of the material. The former is of interest for microwave dielectric applications, whereas the latter may find applications in the photocatalytic splitting of water. Considering both the structural dependencies and variability of the properties of complex niobium oxides, it is of interest to pursue the preparation of new niobate materials. To date, most of the niobates evaluated for their photocatalytic and dielectric properties were typically synthesized via a traditional solid-state technique,[1–4,10,11,14–17] although other methods, such as hydrothermal synthesis[12,18] and flux-aided preparation,[5,9] have been employed; nevertheless, traditional ceramic technique seems to be the most widely used.

As the library of complex niobium oxides with diverse and interesting properties, such as photocatalytic activity and dielectric properties, expands, it becomes ever more important to find new synthetic approaches for the discovery of new materials exhibiting new crystal structures and, therefore, potentially new or enhanced properties. Crystal growth out of molten hydroxides has been shown to be one such approach for the discovery of new materials.[19–21] The acid−base chemistry of molten hydroxide fluxes, best described by the Lux-Flood concept of oxoacidity,[22,23] allows for the dissolution of a wide range of species in molten hydroxides, which is critical for their incorporation into a crystal. On the basis of this concept of oxoacidity, the autodissociation of water (eq 1), and the analogous autodissociation of molten hydroxides (eq 2) yields acid (H_3O^+ and H_2O) and base (OH^- and O^{2-}) species, respectively.

* To whom correspondence should be addressed. Tel.: (803) 777-6916. Fax: (803) 777-8508. E-mail: zurloye@mail.chem.sc.edu.
[†] University of South Carolina.
[‡] University of Florida.

(1) Kan, A.; Ogawa, H.; Yokoi, A.; Nakamura, Y. *J. Eur. Ceram. Soc.* **2007**, *27*, 2977.
(2) Nobre, M. A. L.; Lanfredi, S. *Catal. Today* **2003**, *78*, 529.
(3) Solomon, S.; Joseph, J. T.; Kumar, H. P.; Thomas, J. K. *Mater. Lett.* **2006**, *60*, 2817.
(4) Sebastian, M. T.; Solomon, S.; Ratheesh, R.; George, J.; Mohanan, P. *J. Am. Ceram. Soc.* **2001**, *84*, 1487.
(5) Kharitonova, E. P.; Voronkova, V. I.; Yanovskii, V. K.; Stefanovich, S. Y. *J. Cryst. Growth* **2002**, *237* (239), 703.
(6) Yu, C.; Liu, X.; Yu, M.; Lin, C.; Li, C.; Wang, H.; Lin, J. *J. Solid State Chem.* **2007**, *180*, 3058.
(7) Blasse, G.; Lammers, M. J. J.; Verhaar, H. C. G.; Brixner, L. H.; Torardi, C. C. *J. Solid State Chem.* **1985**, *60*, 258.
(8) Blasse, G. *J. Solid State Chem.* **1988**, *72*, 72.
(9) Walasek, A.; Zych, E.; Zhang, J.; Wang, S. *J. Lumin.* **2007**, *127*, 53.
(10) Abe, R.; Higashi, M.; Zou, Z.; Sayama, K.; Abe, Y.; Arakawa, H. *J. Phys. Chem. B* **2004**, *108*, 811.
(11) Zhang, G.; Gong, J.; Zou, X.; Fangsheng, H.; Zhang, H.; Zhang, Q.; Liu, Y.; Yang, X.; Hu, B. *Chem. Eng. J.* **2006**, *123*, 59.
(12) Zhang, G.; He, F.; Zou, X.; Gong, J.; Tu, H.; Zhang, H.; Zhang, Q.; Liu, Y. *J. Alloys Compd.* **2007**, *427*, 82.
(13) Zhang, G.; Zou, X.; Gong, J.; He, F.; Zhang, H.; Zhang, Q.; Liu, Y.; Yang, X.; Hu, B. *J. Alloys Compd.* **2006**, *425*, 76.
(14) Zou, Z.; Ye, J.; Arakawa, H. *Mater. Res. Bull.* **2001**, *36*, 1185.
(15) Cavazos, R. J.; Schaak, R. E. *Mater. Res. Bull.* **2004**, *39*, 1209.
(16) Muktha, B.; Darriet, J.; Madras, G.; Guru Row, T. N. *J. Solid State Chem.* **2006**, *179*, 3919.
(17) Toda, K.; Honma, T.; Ye, Z.-G.; Sato, M. *J. Alloys Compd.* **1997**, *249*, 256.
(18) Liu, J. W.; Chem, G.; Li, Z. H.; Zhang, Z. G. *Int. J. Hydrogen Energy* **2007**, *13*, 2269.
(19) Davis, M. J.; Mugavero III, S. J.; Glab, K. I.; Smith, M. D.; zur Loye, H.-C. *Solid State Sci.* **2004**, *6*, 413.
(20) Gemmill, W. R.; Smith, M. D.; zur Loye, H.-C. *J. Solid State Chem.* **2006**, *179*, 1750.
(21) Mugavero III, S. J.; Smith, M. D.; zur Loye, H.-C. *J. Solid State Chem.* **2005**, *178*, 200.
(22) Lux, H. Z. *Z. Elektrochem.* **1939**, *45*, 303.
(23) Flood, H.; Forland, T. *Acta Chem. Scand.* **1947**, *1*, 592.

10.1021/cm703479k CCC: $40.75
Published on Web 05/02/2008

$$2H_2O \leftrightarrow H_3O^+ + OH^- \quad (1)$$

$$2\ OH^- \leftrightarrow H_2O + O^{2-} \quad (2)$$

Thus, by analogy with water, where H_3O^+ is the acid and OH^- the base, in a hydroxide melt, H_2O is the acid and O^{2-} is the base. The solubility of metals in molten hydroxides is strongly dependent on the melt's acidity (or water content), which can therefore be used to control the solubility of metal cations[24] and, furthermore, initiate the crystal growth of complex oxides. Our group has successfully developed an effective method for the single-crystal growth of lanthanide-containing oxides of late transition metals utilizing molten hydroxide fluxes.[19–21] However, the area of crystal growth of niobates, tantalates, and other early transition metal oxides using hydroxide fluxes has yet to be explored. Thus, our recent efforts have been focused on the preparation of mixed rare-earth and early transition metal containing complex oxides using a "wet" hydroxide flux route, which has resulted in the successful synthesis of several new complex niobium oxides, namely $La_2KNbO_6$and Nd_2KNbO_6, and the exploration of their properties.

It is known that other complex niobates, such as $LnTiNbO_6$ (Ln = Ce, Pr, Nd, Sm, Eu, Gd, Tb, Y, Yb), possess a high dielectric constant with a positive temperature coefficient of the resonant frequency for the smaller rare earths, whereas a small dielectric constant with a negative temperature coefficient of the resonant frequency was found for compositions containing the larger rare earths.[4] For that reason, the title compound, Ln_2KNbO_6, containing niobium, a rare earth, and an alkali metal cation to affect the dielectric constant and its temperature dependence[1] would seem to be an interesting composition to investigate with respect to its dielectric behavior. The results of this investigation are reported herein.

Another area where niobates are of interest includes the photo-oxidation of organic molecules as well as the photocatalytic splitting of water. During the past years, photocatalysis and its applications in water splitting and wastewater remediation has become one of the fastest growing areas of research. An increased interest in semiconducting oxides as possible candidates for photocatalytic processes began with the study of TiO_2 by Honda and Fujishima.[25] Since then, complex semiconducting oxides of titanium, niobium, and tantalum have shown promise for photocatalytic applications[10,11,13–15,18] and have taken a prominent place among the candidates for the efficient photocatalytic splitting of water as well as for wastewater remediation. Much attention has focused on complex niobium oxides with layered structures containing NbO_6 octahedral units, because it had been postulated that octahedral coordination of niobium within a complex structure is responsible for the diverse properties of the material.[12,18] However, unusual coordination environments for niobium and photocatalytic activity of the materials containing those units have not been well studied. Even though such materials exist, for example, $NaRbLnNbO_5$ (Ln = La, Nd, Sm, Eu, Gd),[15] they have not been studied for their photocatalytic activity. The title compounds containing niobium in a rare square pyramidal coordination environment are of interest for the investigation of their photocatalytic abilities.

Herein, we report on the single crystal growth of two new complex niobates, $La_2KNbO_6$and Nd_2KNbO_6, utilizing reactive hydroxide fluxes, and on their structure determination and investigation of their dielectric, photocatalytic, and photophysical properties.

Experimental Section

Sample Preparation. Crystals of La_2KNbO_6 and Nd_2KNbO_6 were grown out of molten KOH containing approximately 15% water by weight. 1.00 mmol of the respective lanthanide sesquioxides, Ln_2O_3 (Alfa Aesar, REacton, 99.9%) prefired at 1000 °C for 24 h, 1 mmol of Nb_2O_5 (Alfa Aesar, 99.9%) and 3 g of KOH (Fisher, ACS grade) were loaded into a silver tube (10 cm long, 1.25 cm diameter), which had been flame sealed at one end. For the preparation of Nd_2KNbO_6, an additional 1 g of $KF \cdot 2H_2O$ (Alfa Aesar, 98.5+%) and 1 g of deionized water were added to the reaction mixture. The silver tube was crimped shut on the other end and folded over three times before being placed upright in a box furnace. Synthetic conditions were optimized to obtain the highest quality single crystals of both members of the family. For La_2KNbO_6, the system was heated to 600 °C in 2 h, and held at the target temperature for 24 h. At that point, the furnace was shut off, allowing for the system to cool to room temperature. For Nd_2KNbO_6, the reaction was carried out at 500 °C for 24 h and subsequently cooled to 200 °C over 30 h, at which point the system was cooled to room temperature by shutting off the furnace. Elongated hexagonal, clear-transparent crystals of La_2KNbO_6 and rodlike, blue transparent crystals of Nd_2KNbO_6 were isolated by dissolving the flux with water aided by sonication.

Characterization. *Single-Crystal X-ray Diffraction.* X-ray diffraction intensity data from a colorless plate crystal of La_2KNbO_6 and from a pale blue needle crystal of Nd_2KNbO_6 were measured at 294(2) K on a Bruker SMART APEX diffractometer (Mo Kα radiation, $\lambda = 0.71073$ Å).[26] The data collection covered 99.5% of reciprocal space to $2\theta = 70.6°$ (average redundancy = 4.4, $R_{int} = 0.031$) for La_2KNbO_6 and 99.9% of reciprocal space to $2\theta = 70.6°$ (average redundancy = 5.2, $R_{int} = 0.042$) for Nd_2KNbO_6. Raw area detector data frame integration was performed with SAINT+.[26] Final unit-cell parameters were determined by least-squares refinement of 4030 reflections from the data set of La_2KNbO_6 and 3470 reflections from the data set of Nd_2KNbO_6. An absorption correction based on multiple measurements of equivalent reflections was applied to the data with SADABS.[26] Direct methods structure solution, difference Fourier calculations and full-matrix least-squares refinement against F^2 were performed with SHELXTL.[27]

The compounds crystallize in the space group *C*2/*m* as determined by the pattern of systematic absences in the intensity data and by the successful solutions and refinements of the structures. The structural model for Nd_2KNbO_6 was derived from the isostructural La analog and was refined by full-matrix least-squares against F^2 with SHELXTL.[27] Convergence was rapidly achieved.

There are eight atoms in the asymmetric unit: two independent lanthanum or neodymium atoms, one niobium atom, one potassium atom and four oxygen atoms. All metal atoms and oxygen O1 reside on crystallographic mirror planes (Wyckoff site 4i). O2 and O3 are on general positions (site 8j) and O4 lies on a 2-fold axis of

(24) Keller, S. W.; Carlson, V. A.; Sandord, D.; Stenzel, F.; Stacy, A. M.; Kwei, G. H.; Alario-Franco, M. *J. Am. Chem. Soc.* **1994**, *116*, 8070.
(25) Fujishima, A.; Honda, K. *Nature* **1972**, *238*, 37.
(26) *SMART V. 5.625, SAINT 22 V. 6.45, and SADABS V. 2.05*; Bruker Analytical X-ray Systems, Inc.: Madison, WI, 2001.
(27) *SHELXTL V. 6.14*; Bruker Analytical X-ray Systems, Inc.: Madison, WI, 2000.

Table 1. Crystal Data and Structural Refinement for La_2KNbO_6 and Nd_2KNbO_6

empirical formula	La_2KNbO_6	Nd_2KNbO_6
fw (g mol^{-1})	505.83	516.49
space group	*C2/m*	*C2/m*
a (Å)	12.7460(2)	12.5455(3)
b (Å)	5.7906(1)	5.6985(1)
c (Å)	8.8719(2)	8.7196(2)
β (deg)	105.965(1)	105.803(1)
V ($Å^3$)	629.55(2)	599.81(2)
Z	4	4
D_{calcd} (g cm^{-3})	5.337	5.720
abs coeff (mm^{-1})	15.741	19.590
F (000)	888	912
cryst size (mm^3)	0.12 × 0.08 × 0.02	0.08 × 0.03 × 0.02
θ range	2.39–35.32	2.43–35.30
no. of reflns collected	6848	7549
no. of independent reflns	1532(R_{int} = 0.0310)	1459(R_{int} = 0.0416)
GOF on F^2	1.072	1.090
R indices (all data)	R_1 = 0.0222 wR_2 = 0.0461	R_1 = 0.0266 wR_2 = 0.0513
largest diffraction peak and hole (e^- $Å^{-3}$)	1.134 and −1.404	1.619 and −1.920

Table 2. Atomic Coordinates and Equivalent Isotropic Displacement Parameters for La_2KNbO_6 and Nd_2KNbO_6

	x	*y*	*z*	U_{eq}
		La_2KNbO_6		
La1	0.3699(1)	1/2	0.0718(1)	0.008(1)
La2	0.0899(1)	1/2	0.2071(1)	0.008(1)
Nb1	0.3416(1)	0	0.2979(1)	0.007(1)
K1	0.1148(1)	0	0.4809(1)	0.015(1)
O1	0.3228(2)	0	0.4945(3)	0.013(1)
O2	0.2373(1)	0.2308(3)	0.1698(2)	0.011(1)
O3	0.4508(1)	0.2296(3)	0.2950(2)	0.010(1)
O4	0	0.2525(4)	0	0.010(1)
		Nd_2KNbO_6		
Nd1	0.3704(1)	1/2	0.0705(1)	0.007(1)
Nd2	0.0888(1)	1/2	0.2038(1)	0.007(1)
Nb1	0.3416(1)	0	0.2975(1)	0.007(1)
K1	0.1153(1)	0	0.4784(1)	0.013(1)
O1	0.2355(3)	0	0.4992(4)	0.012(1)
O2	0.2358(2)	0.2338(4)	0.1682(3)	0.011(1)
O3	0.4518(2)	0.2322(4)	0.2923(3)	0.009(1)
O4	0	0.2501(5)	0	0.009(1)

rotation (site 4g). All atoms were refined with anisotropic displacement parameters. For La_2KNbO_6, the largest residual electron density extrema are +1.13 and −1.40 $e^-/Å^3$, located 0.68 and 0.70 Å from La2 and La1, respectively. For Nd_2KNbO_6, the largest residual electron density extrema are +1.62 and −1.92 $e^-/Å^3$, located 0.69 and 0.63 Å from Nd1 and Nb1, respectively.

Relevant crystallographic data from the single-crystal structure refinements for Ln_2KNbO_6 (Ln = La, Nd) are found in Table 1. Atomic positions, selected interatomic distances, and bond angles are summarized in Tables 2 and 3, respectively.

Further details of the crystal structure investigations can be obtained from the Fachinformationszentrum Karlsruhe, 76344 Eggenstein-Leopoldshafen, Germany; fax, +49 7247 808 666; e-mail, crystdata@FIZ-Karlsruhe.de on quoting the depository numbers CSD- 418875 for La_2KNbO_6 and CSD-418874 for Nd_2KNbO_6.

Powder X-ray Diffraction. Powder X-ray diffraction measurements were performed using a Rigaku D/Max 2100 monochromatized Cu *K*α radiation equipped with a hot stage and. Data were collected in 0.04 ° steps over the two-theta range of 5−80°. Data were collected between 298 and 1273 K. The temperature was held for 30 min at each target temperature to allow for thermal equilibration before data were collected.

Scanning Electron Microscopy. Environmental scanning electron micrographs of single crystals of both compounds were obtained using the low vacuum mode of an FEI Quanta 200 ESEM instrument. Energy-dispersive spectroscopy (EDS) verified the presence of lanthanides (lanthanum and neodymium for La_2KNbO_6 and Nd_2KNbO_6 respectively), potassium, niobium, and oxygen. Within the detection limit of the instrument, no other elements were observed.

Table 3. Selected Interatomic Distances (Å) and Bond Angles (deg) for La_2KNbO_6 and Nd_2KNbO_6

	La_2KNbO_6	Nd_2KNbO_6
Ln(1)−O(4) (×2)	2.4237(15)	2.3659(19)
Ln(1)−O(3) (×2)	2.5126917)	2.457(2)
Ln(1)−O(2) (×2)	2.5761(18)	2.524(2)
Ln(1)−O(2) (×2)	2.6172(18)	2.581(2)
Ln(2)−O(4) (×2)	2.3629(15)	2.3127(19)
Ln(2)−O(3) (×2)	2.5063(18)	2.45492)
Ln(2)−O(2) (×2)	2.5324(17)	2.471(2)
Ln(2)−O(1)	2.575(2)	2.519(3)
Nb−O(1)	1.825(2)	1.825(3)
Nb−O(3) (×2)	1.9300(17)	1.923(2)
Nb−O(2) (×2)	2.0028(17)	1.999(2)
K−O(1)	2.620(3)	2.594(3)
K−O(3) (×2)	2.7653(18)	2.712(2)
K−O(3) (×2)	2.8320(19)	2.820(2)
K−O(1) (×2)	2.9944(7)	2.9378(9)

TGA/DTA. The TGA/DTA measurements were performed using a TA Instruments SDTQ 600 simultaneous TGA/DTA to study possible phase transitions as a function of temperature, as well as the thermal stability of La_2KNbO_6 at elevated temperatures. The measurements were performed on ground crystals of La_2KNbO_6. The powder sample was heated from 25 to 1200 °C using a constant gas flow of air, 100 cc/min.

UV−Visible Spectrometry. The diffuse-reflectance spectrum of ground crystals of La_2KNbO_6 was obtained using a Shimadzu UV/vis NIR Scanning Spectrophotometer UV 3101 (PC) equipped with an integrating sphere. The spectrum was converted from reflection to absorbance using the Kubelka−Munk method. The optical band gap energy was calculated using the onset of the absorption edge. The spectrum is shown in Figure 4. It was not possible to synthesize a pure sample of Nd_2KNbO_6 to perform the UV−vis measurements, as crystals of Nd_2O_3 were intimately mixed with crystals of the target compound, Nd_2KNbO_6. For comparison, the diffuse reflectance spectrum of Degussa P-25 TiO_2 was collected utilizing a Perkin-Elmer UV/vis Scanning Spectrophotometer Lambda 35 (PC) equipped with an integrating sphere. The spectrum was converted from reflection to absorbance using the Kubelka−Munk function.

Photoluminescence and Semiempirical PM6 Calculations. Photoexcited luminescence spectra were recorded using a Fluorat-02-Panorama spectrofluorimeter system, using an excitation wavelength of 260 nm and emission wavelength of 415 nm. The experiments were performed at room temperature using ground crystals of La_2KNbO_6. The semiempirical PM6 calculations were performed using MOPAC2007,[28] with periodic boundary conditions and geometries obtained from the single crystal X-ray diffraction data.

Dielectric Measurements. Dielectric measurements were performed in air on a polycrystalline ceramic sample of La_2KNbO_6 over the temperature range of 123−473 K, using four different frequencies. Phase pure powder of La_2KNbO_6 was uniaxially pressed into a disk-shaped pellet (8 mm diameter and 2 mm thickness) using polyvinyl alcohol (∼1%) as a binder under a pressure of 180 MPa. Subsequently, the pellet was cold pressed isostatically at 300 MPa for 30 min. The extended pressing time was used to achieve a high-density green ceramic pellet. Because La_2KNbO_6 undergoes a phase transition to La_3NbO_7 above 1273

(28) Stewart, J. P. *MOPAC 2007*; Stewart Computational Chemistry: Colorado Springs, CO, 2007.

K, sintering temperatures were limited to 900 K; thus, the ceramic pellet of La_2KNbO_6 was sintered at 873 K for 80 h. The geometrical density of the sintered pellet was measured to be approximately 58% of theoretical density; clearly an indication that the polycrystalline sample was not completely sintered. While different heat treatment and sintering profiles were also tested, none resulted in higher densification.

The sintered ceramic pellet of La_2KNbO_6 was polished to obtain a planar surface. Silver paste (Alfa-Aesar) was brushed onto both sides of the disk-shaped pellet to serve as the electrode. The silver coated ceramic pellet was placed inside a computer controlled Delta 9023 oven and the temperature-dependence of the dielectric properties was measured as a function of frequency (100, 300, 800, and 1000 kHz) using an Agilent 4284A precision LCR meter over the temperature range of 123−473 K. Because the sample was highly porous, the measured dielectric permittivity was corrected for porosity using Wakino's approximations.[30]

Photocatalytic Activity Measurements. The decoloration of methylene blue (MB) (2×10^{-5} M) was used as a screening method for the initial evaluation of the photocatalytic activity of La_2KNbO_6 under ultraviolet light using a 150 W Xe lamp as the ultraviolet light source. The pellet of a sample was placed at the bottom of a disposable cuvette (UV grade polymethylmethacrylate PMMA, 280−800 nm) containing 3 mL of MB. The distance from the light source to the cuvette was 10 in. and the experiment was performed at room temperature. No convection was introduced during these experiments. Ultraviolet−visible spectroscopy was used to monitor the MB decoloration between 400 and 800 nm by following the absorption doublet located around 660 nm as a function of time. Ultraviolet−visible data were collected using a Fluorat-02-Panorama spectrofluorometer.

Results and Discussion

Crystal Structure. Hydroxides are known to be an excellent medium for preparing single crystals of lanthanide-containing complex oxides.[19–21,24] In the case of both La_2KNbO_6 and Nd_2KNbO_6, the Lux-Flood acidic (water rich) KOH flux acted as both solvent and reactant. Because controlling the acidity of the melt is an essential component to the successful dissolution and subsequent recrystallization of the constituents, the dehydration of the melt was minimized by conducting the crystal growth process in sealed silver tubes. In the case of Nd_2KNbO_6, additional water was required to adjust the pH_2O of the melt to promote dissolution of the reactant species and, subsequently, to facilitate the crystallization of the product. The limiting conditions for the dissolution of niobium and other early transition metals in hydroxide fluxes are yet to be determined. However, as we have established on the basis of our initial results, the dissolution of Nb(V) and Ta(V) can be achieved in acidic hydroxide fluxes. The SEM micrographs of elongated hexagons of La_2KNbO_6 and rodlike crystals of Nd_2KNbO_6 are shown in images a and b in Figure 1, respectively. Both La_2KNbO_6 and Nd_2KNbO_6 crystallize in the monoclinic space group $C2/m$, with $a = 12.7460(2)$ and $12.5455(3)$ Å, $b = 5.7906(1)$ and $5.6985(1)$ Å, $c = 8.8719(2)$ and $8.7196(2)$ Å, $\beta = 105.965(1)$ and $105.803(1)°$ for lanthanum and neodymium analogs, respectively.

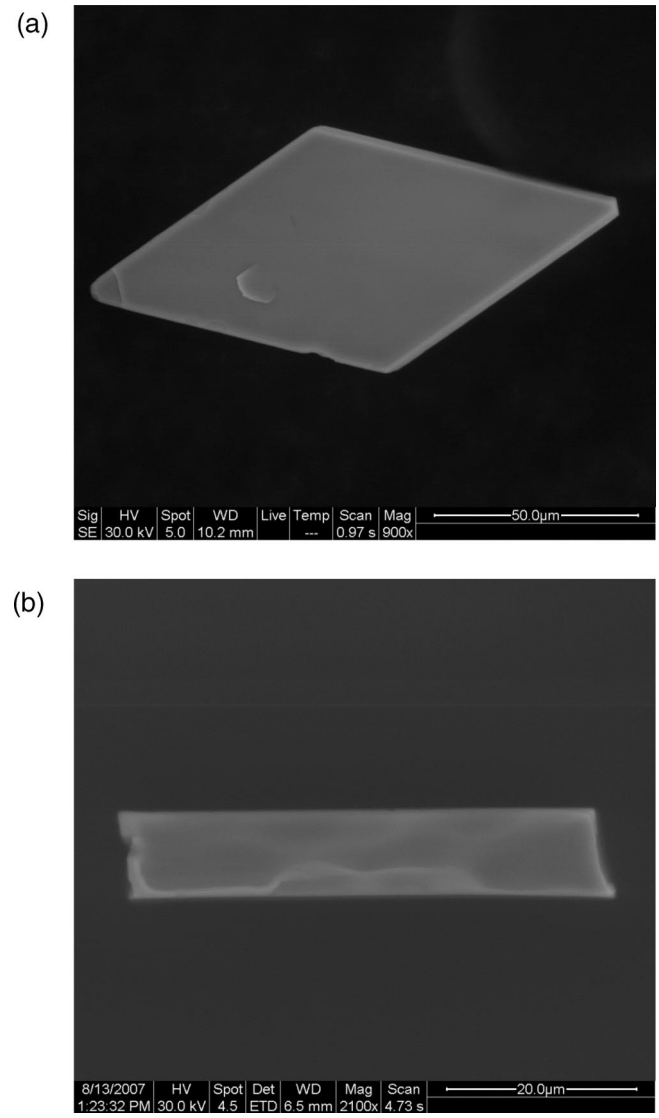

Figure 1. ESEM images of single crystals of (a) La_2KNbO_6 and (b) Nd_2KNbO_6 grown out of the reactive hydroxide flux.

La_2KNbO_6 and Nd_2KNbO_6 crystallize in a new crystal structure type, the schematic of which is shown in Figure 2. The structure is best thought of as consisting of pseudolayers of interconnected LnO_8 and LnO_7 polyhedra. Niobium atoms are isolated in NbO_5 square pyramids, which at the base are edge-shared to the three LnO_8 distorted cubes and one LnO_7 polyhedron and at the apex are connected to the LnO_7 polyhedron from the next layer. The 7-coordinate potassium atoms are located in the cavities of the Ln_2NbO_6 slabs. Figure 3 shows the structure viewed along the z-axis. The potassium polyhedra are connected within the interlayer and also connected to the Ln_2NbO_6 slabs through the vertices of the NbO_5 square pyramids located in an adjacent layer. This pseudolayered structure suggests the possibility of modifying the chemical composition of the material through ion exchange of the potassium atoms. However, all attempts at exchanging the potassium ion with Li and Na were unsuccessful. The preparation of other compositions incorporating smaller rare earth cations was also attempted; however, neodymium appears to be the smallest rare earth that the structure will accommodate. All attempts to incorporate a smaller rare earth ion into the structure were unsuccessful.

(29) Serafin, M.; Hoppe, R. *Rev. Chim. Mineral.* **1983**, *20*, 214.
(30) Surble, S.; Obbade, S.; Saad, S.; Yagoubi, S.; Dion, C.; Abraham, F. *J. Solid State Chem.* **2006**, *179*, 3258.

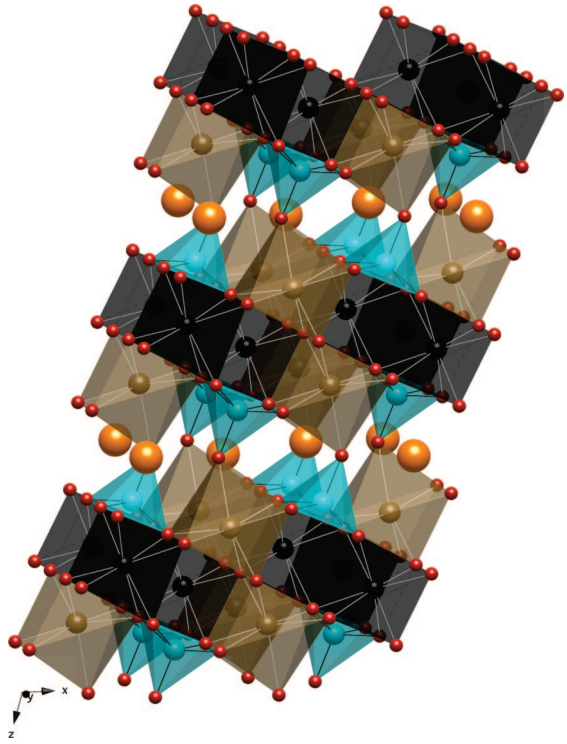

Figure 2. Schematic of the crystal structure of La_2KNbO_6. 7- and 8-coordinate La^{3+} ions are shown in brown and black, respectively. NbO_5 polyhedra are shown in blue. Potassium atoms are shown as large orange spheres and oxygen atoms as small red spheres.

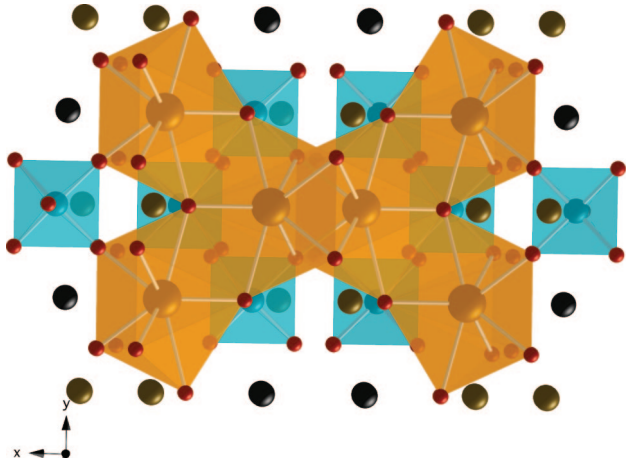

Figure 3. Schematic depiction of the interconnected potassium polyhedra between the slabs of La_2NbO_6along the *z*-axis. The KO_7 polyhedra are shown in orange; NbO_5 square pyramids are in blue; LnO_7 and LnO_8 are shown as brown and black spheres, respectively. Oxygen atoms are red spheres.

An interesting and unusual feature of this novel, pseudolayered structure is the square pyramidal coordination environment of the niobium atoms. Although 5-coordinate niobium has been observed before, e.g., in $NaRbLnMO_5$ (Ln = La − Gd; M = Nb, Ta),[15] $Rb_4Nb_6O_{17}$,[29] $A_{1-x}UNbO_{6-x/2}$ (x = 0, A = Li, Na K, Cs and x = 0.5, A = Rb, Cs),[30] $Na_{13}Nb_{35}O_{94}$,[31] and $LaKNaNbO_5$,[32] it is not very common in solid-state structures. The square pyramidal coordination environment around the central niobium atom in Ln_2KNbO_6 is slightly distorted, with basal bond distances of Nb1−O2 (2.0028(17) and 1.999(2) Å), Nb1−O3 (1.9300(17) and 1.923(2) Å), and apical bonds of Nb1−O1 (1.825(2) and 1.825(3) Å) for the lanthanum and niobium analogs, respectively (Table 3). In addition, the niobium atom is situated slightly above the crystallographic plane of the four oxygens that make up the distorted base of the "square" pyramid.

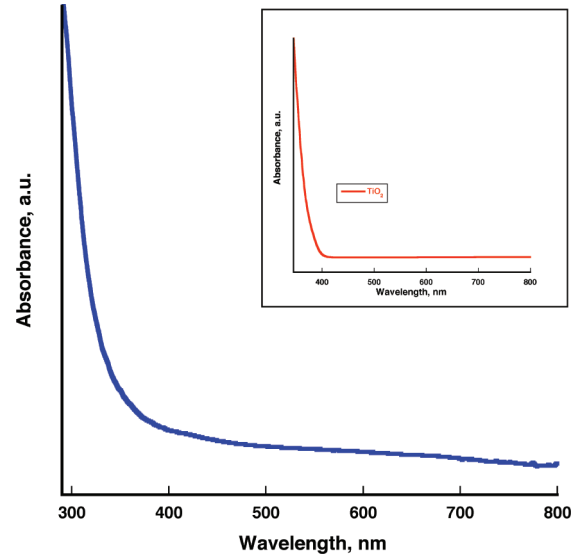

Figure 4. UV−vis diffuse reflectance spectrum of La_2KNbO_6. The inset shows the UV−vis diffuse reflectance spectrum of Degussa P-25 TiO_2.

Photocatalytic and Photophysical Properties. *Absorption Spectra.* Figure 4 shows the diffuse reflectance spectrum collected using ground crystals of La_2KNbO_6. The material has a large absorption edge corresponding to the energy gap between the filled oxygen 2p band and the empty conduction band (vide infra). The spectrum represents the typical optical response of a wide-band gap semiconductor with absorption beginning at about 400 nm, corresponding to a band gap energy of ~3.1 eV. For comparison, the absorption spectrum of Degussa P-25 TiO_2, a standard for photocatalytic measurements, is shown in the inset of Figure 4. The absorption edge for P-25 is located around 380 nm, which corresponds to a band gap of 3.2 eV. To evaluate the potential of La_2KNbO_6 for photocatalytic applications, the photocatalytic degradation of methylene blue was investigated.

Photocatalytic Activity for Degradation of Methylene Blue. UV−vis Spectral Changes. La_2KNbO_6 is photocatalytically active under UV irradiation. Figure 5a shows the changes in the absorption spectra of a methylene blue solution as a function of time during irradiation by a UV lamp (150 W Xe). Initially two peaks are observed at 612 and 661 nm. As the experiment progresses, the peak positions do not shift, indicating that the structure of methylene blue does not change; however, the peak intensity decreases, indicating that the concentration of methylene blue is decreasing due to decomposition. For comparison, Figure 5b shows changes in the absorption spectra of methylene blue solution as a function of time when P-25 TiO_2 is used as the photocatalyst. Clearly, the methylene blue peak at 612 nm decreases in intensity, indicating the degradation of the dye in the solution. Figure 5c shows the absorption spectra for methylene blue solution when La_2KNbO_6 is used as the photocatalyst. La_2KNbO_6, even though photocatalytically active as indicated by the decrease in the concentration of methylene

(31) Craig, D. C.; Stephenson, N. C. *J. Solid State Chem.* **1971**, *3*, 89.
(32) Liao, J.-H.; Tsai, M.-C. *Cryst. Growth Des.* **2002**, *2*, 83.

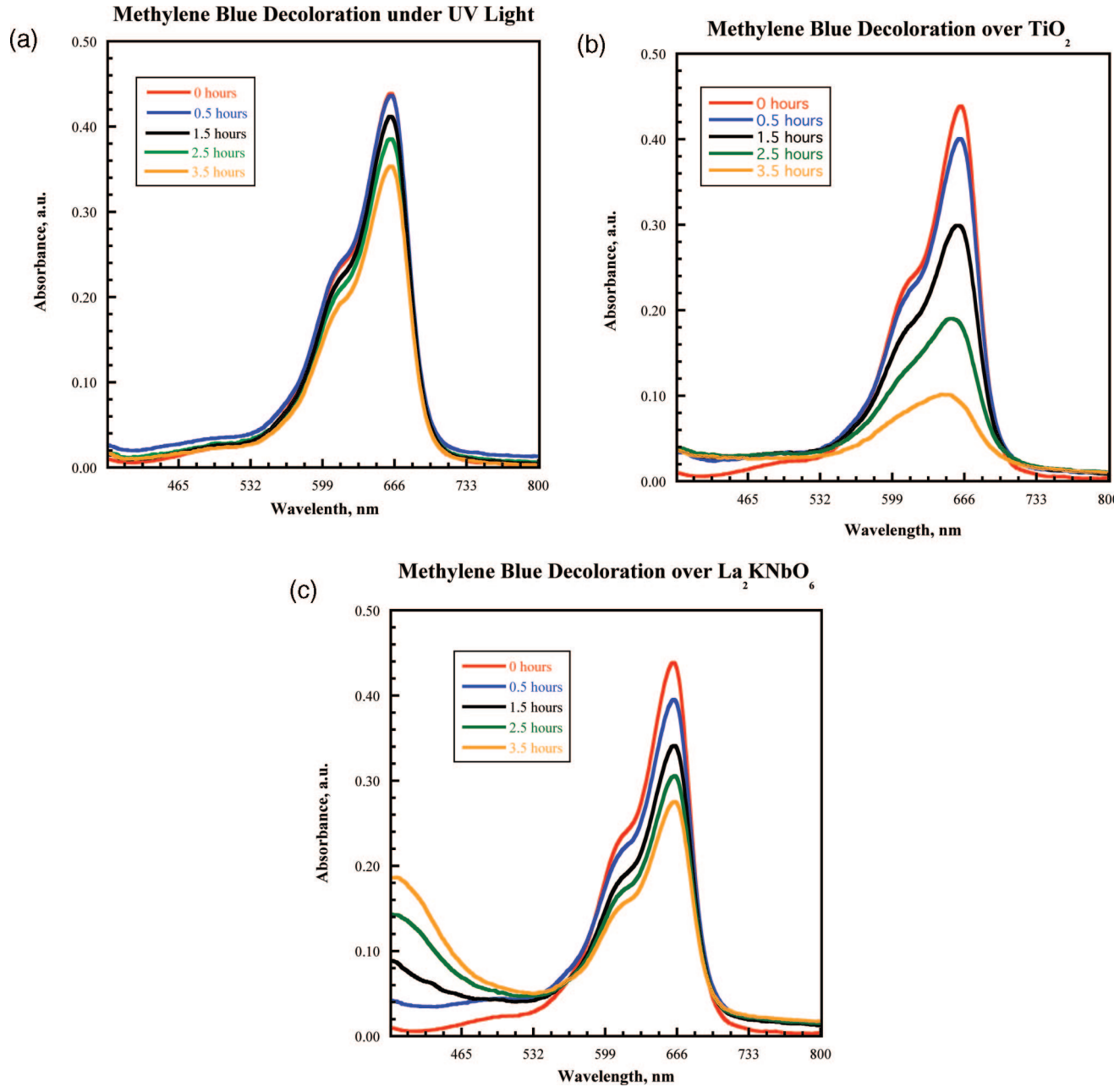

Figure 5. (a) Changes in the UV−vis spectra during the photocatalytic degradation of methylene blue solution with no catalyst. (b) Changes in the UV−vis spectra during the photocatalytic degradation of methylene blue solution over TiO_2 (Degussa, P-25). (c) Changes in the UV−vis spectra during the photocatalytic degradation of methylene blue solution over La_2KNbO_6.

blue dye in the solution, does not degrade the dye completely. Interestingly, there is an extra peak at 402 nm, which increases with time, suggesting that methylene blue is not being degraded completely, but rather converted into a new species that absorbs at 402 nm. After the UV irradiation, the methylene blue solution had a green tint, which is consistent with the presence of two solution species having absorption peaks at 402 and 612 nm, respectively. Undoubtedly, although additional studies are required to thoroughly explain the photoinduced processes within the system, we can nonetheless conclude that La_2KNbO_6 has some photocatalytic activity toward the degradation of methylene blue.

The difference in the activity of two catalysts, TiO_2 and La_2KNbO_6, can be explained through the comparison of the surface areas of the materials, which influences a material's photocatalytic activity. P-25 TiO_2 is a high surface area material (50 m^2/g),[33] whereas single crystals of La_2KNbO_6 had to be ground to perform the measurement, resulting in a surface area of less than 1 m^2/g. However, attempts to prepare La_2KNbO_6 by other methods, such as traditional ceramic, hydrothermal, and Pechini syntheses to obtain a high-surface-area material, were unsuccessful. At higher temperatures, La_2KNbO_6 decomposes into La_3NbO_7 plus other unidentifiable oxide species. All syntheses carried out at temperatures above 600 °C lead to the formation of predominantly La_3NbO_7 instead of La_2KNbO_6. To identify the structural transition of La_2KNbO_6, we collected powder X-ray diffraction data at elevated temperatures. The powder X-ray diffraction patterns collected as a function of temper-

(33) Krysa, J.; Keppert, M.; Jirkovsky, J.; Stengl, V.; Subrt, J. *Mater. Chem. Phys.* **2004**, *86*, 333.

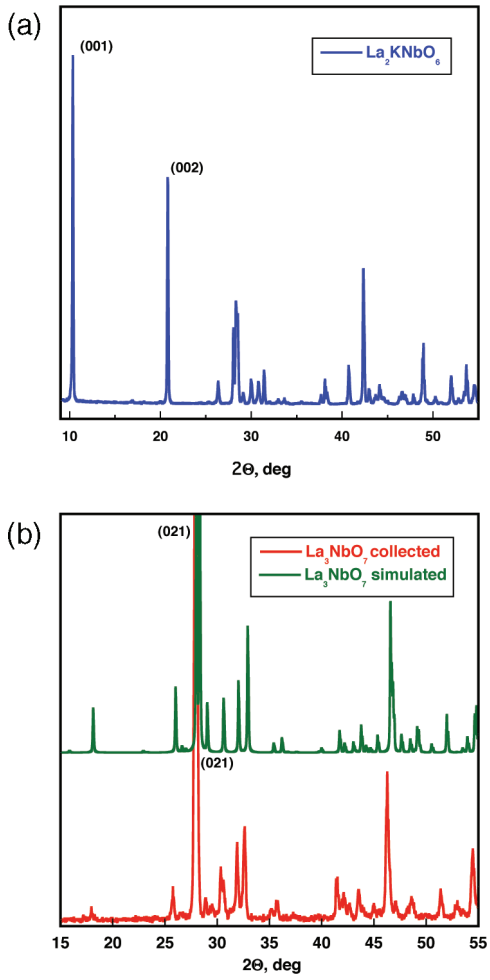

Figure 6. (a) XRD pattern of La_2KNbO_6 collected at room temperature; (b) XRD patterns collected at 1273 K (red) and calculated room temperature pattern for La_3NbO_7 (green).

ature are shown in Figure 6, where the decomposition of La_2KNbO_6 and the formation of La_3NbO_7 can clearly be seen at 1000 °C. The pattern collected at room temperature (Figure 6a) shows distinct (001) and (002) peaks characteristic of the pseudolayered structure of La_2KNbO_6. However, when collected at 1000 °C (Figure 6b), those prominent peaks disappear, whereas the (021) peak of La_3NbO_7 becomes more intense. Data collected at high temperature were fitted to the La_3NbO_7 lattice parameters using the Le Bail extraction method revealing a clear match. The calculated pattern of La_3NbO_7 is shown in green in Figure 6b for comparison.

Photoluminescence. The photoluminescence of La_2KNbO_6 was investigated both experimentally and theoretically. Figure 7 shows the room temperature excitation and emission spectra of La_2KNbO_6. The broad emission band has its maximum at 424 nm with the corresponding excitation band at 260 nm. For visual comparison, Figure 8 shows optical pictures of the ground La_2KNbO_6 crystals (a) under incandescent light and (b) under UV irradiation. When exposed to the short wavelength UV irradiation, the compound emits a blue-violet light as seen on the optical pictures.

To help explain the photoluminescence of La_2KNbO_6, we carried out semiempirical PM6 calculations. These calculations provide a model for the HOMO−LUMO separation and explain the presence of an isolated state within the

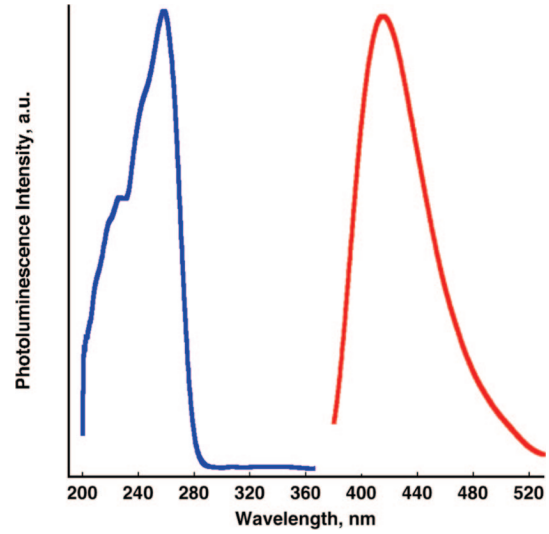

Figure 7. Room-temperature photoluminescence spectrum of La_2KNbO_6.

electronic structure of the compound, which is responsible for the intense blue-violet emission. It is well-known that orbital energy differences strongly overestimate actual excitation energies, and either configuration interaction or time dependent treatments are needed to model the energetics of the electronic excitations. Nevertheless, the orbital energies provide a useful qualitative description. A schematic of the emission process is shown in Figure 9. The calculations of the electronic structure of La_2KNbO_6 imply that the electrons, when excited into the LUMO+n by the photon absorption, are then relaxed into the isolated LUMO energy level through a nonradiative transition. In the LUMO state, the electrons are localized and do not easily migrate to nonradiative quenching sites, resulting in large relaxation time and de-excitation to the ground state with blue light emission.

The calculations show that the HOMO is mostly O 2p orbital based, whereas the LUMO and LUMO+n are La 6p and O 2s orbital based. The Nb 4p orbitals are too high in energy and do not contribute to the LUMOs. Thus it appears that the contribution of the lanthanum in the material plays an important role in the intense room temperature photoluminescence.

Dielectric Properties. The dielectric permittivity of La_2KNbO_6 was measured as a function of frequency from 100 kHz to 1 MHz. The sample pellets were not at their theoretical density, and therefore, the measured dielectric permittivity was corrected for porosity. Wakino[34] has shown that for a highly porous material (relative porosity above 40%), the following empirical relationship can be used to predict the correct dielectric permittivity

$$\varepsilon_c^{V_m - V_c} = V_m \varepsilon_m^{V_m - V_c} + V_a \varepsilon_a^{V_m - V_c} \quad (3)$$

where ε_c, ε_m, and ε_a are the permittivity of the porous sample, material (La_2KNbO_6), and air, respectively, V_m and V_a are the volume fraction of the material and porosity (air), respectively, and V_c is the constant with a value of 0.35.

If the dielectric permittivity of air ($\varepsilon_{air} = 1$) is input in the above relationship, then eq 1 transforms to

(34) Wakino, K.; Okada, T.; Yoshida, N.; Tomono, K. *J. Am. Ceram. Soc.* **1993**, *76*, 2588.

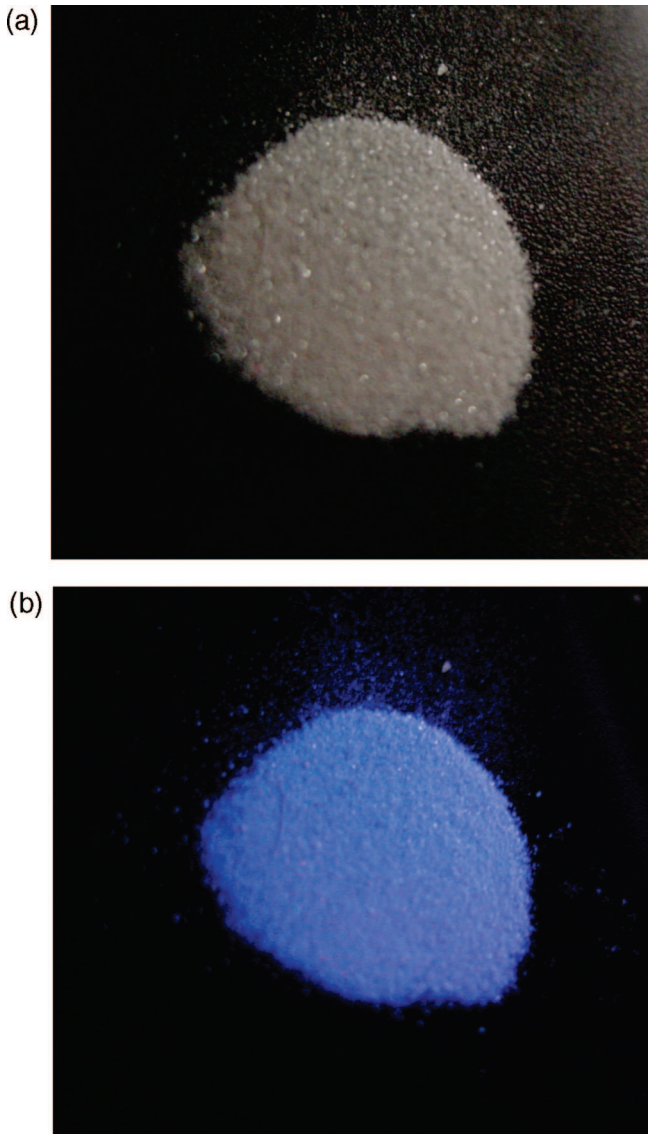

Figure 8. Optical images of La_2KNbO_6 under (a) incandescent light and (b) UV irradiation.

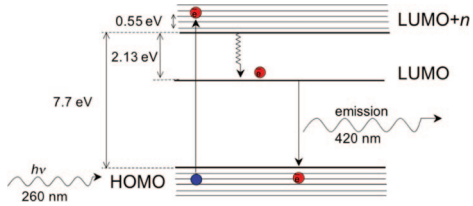

Figure 9. Schematic of the luminescence processes in La_2KNbO_6.

$$\varepsilon_m = \left[\frac{\varepsilon_c^{V_m - V_c} - V_a}{V_m}\right]^{\frac{1}{V_m - V_c}} \quad (4)$$

In the present work, ε_m is reported as the dielectric permittivity of La_2KNbO_6 for different temperatures. Panels a and b in Figure 10 show the real part of the relative permittivity (ε'_r) and the loss (tan δ) of La_2KNbO_6 as a function of temperature at different frequencies.

The ε'_r increases with increasing temperatures for all the measured frequencies. This positive temperature coefficient of the relative permittivity is consistent with the presence of a high temperature phase transition, as indicated by the

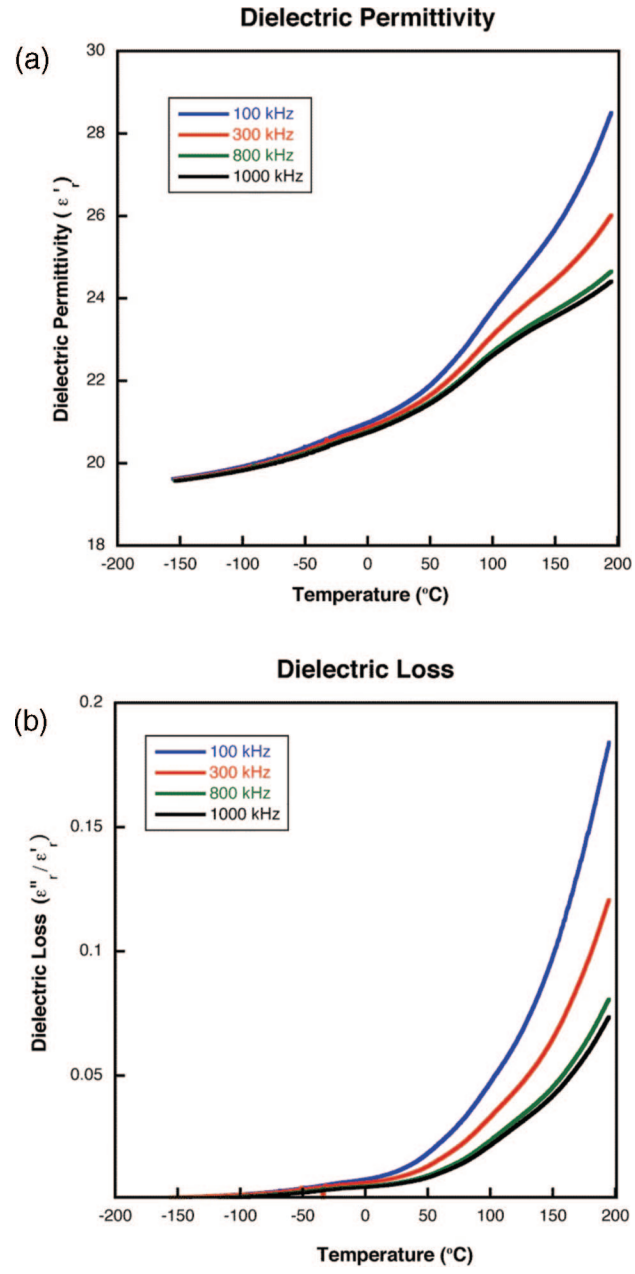

Figure 10. (a) Real part of the relative permittivity and (b) the dielectric loss of La_2KNbO_6ceramic measured at different frequencies as a function of temperature.

TGA and XRD analyses. At low temperatures, the loss remains constant and is around 5×10^{-4}, whereas above 350 K, the upturn in the real part of the permittivity and the sharp increase in tan δ for all the frequencies is indicative of the onset of electrical conduction within the sample, perhaps because of the increased mobility of the potassium ion combined with the porosity of the measured sample.

The low loss and intermediate permittivity make this a material of potential interest for dielectric applications. However, the high-temperature conductivity combined with the limited sinterability, will probably preclude its utilization. Nonetheless, similar compounds, such as those based on tantalum, or structural analogs containing Li or Na, may not undergo a phase transition and may exhibit more stable properties at high temperatures.

Conclusion

We utilized a low-temperature approach to single crystal growth of niobates and successfully prepared two new niobates, La_2KNbO_6 and Nd_2KNbO_6. Both compounds crystallize in a new pseudolayered structure type, which accommodates niobium in an unusual 5-coordinate environment. We characterized La_2KNbO_6 with respect to its photocatalytic activity where the low surface area of the material is mostly responsible for its relatively low photocatalytic activity toward the degradation of methylene blue; nonetheless, the new material is photocatalytically active. In addition, La_2KNbO_6 exhibits room-temperature photoluminescence with a bright blue emission that was rationalized by semiempirical calculations. Although the new La_2KNbO_6 was found to have very limited solid-state sinterability, its dielectric permittivity (corrected for porosity) was measured as $\sim$21 with low loss up to 350 K. Finally, additional calculations need to be performed to obtain more quantitative information about the band structure of La_2KNbO_6 and to draw conclusions about the relationship between the novel structure and the photocatalytic and dielectric properties.

Acknowledgment. This work was supported by the National Science Foundation through Grant DMR:0450103. J.N. acknowledges the financial support of the National Science Foundation through the CAREER Award (DMR-0449710).

CM703479K